LETTER

doi:10.1038/nature14253

Liquid-based gating mechanism with tunable multiphase selectivity and antifouling behaviour

Xu Hou[1,2], Yuhang Hu[1], Alison Grinthal[1], Mughees Khan[2] & Joanna Aizenberg[1,2]

Living organisms make extensive use of micro- and nanometre-sized pores as gatekeepers for controlling the movement of fluids, vapours and solids between complex environments. The ability of such pores to coordinate multiphase transport, in a highly selective and subtly triggered fashion and without clogging, has inspired interest in synthetic gated pores for applications ranging from fluid processing to 3D printing and lab-on-chip systems[1–10]. But although specific gating and transport behaviours have been realized by precisely tailoring pore surface chemistries and pore geometries[6,11–17], a single system capable of controlling complex, selective multiphase transport has remained a distant prospect, and fouling is nearly inevitable[11,12]. Here we introduce a gating mechanism that uses a capillary-stabilized liquid as a reversible, reconfigurable gate that fills and seals pores in the closed state, and creates a non-fouling, liquid-lined pore in the open state. Theoretical modelling and experiments demonstrate that for each transport substance, the gating threshold—the pressure needed to open the pores—can be rationally tuned over a wide pressure range. This enables us to realize in one system differential response profiles for a variety of liquids and gases, even letting liquids flow through the pore while preventing gas from escaping. These capabilities allow us to dynamically modulate gas–liquid sorting in a microfluidic flow and to separate a three-phase air–water–oil mixture, with the liquid lining ensuring sustained antifouling behaviour. Because the liquid gating strategy enables efficient long-term operation and can be applied to a variety of pore structures and membrane materials, and to micro- as well as macroscale fluid systems, we expect it to prove useful in a wide range of applications.

Our hypothesis that a liquid-filled pore could provide a unified gating strategy derives from the idea that a liquid stabilized inside a micropore offers a unique combination of dynamic and interfacial behaviours, and is inspired by nature's use of fluids as reconfigurable gates. Microscale stomata and xylem control air, water and microbe exchange in plants by using liquid to mechanically reconfigure the pore[18]. The nuclear pore is directly lined with disordered, fluid-like proteins that are believed not only to regulate differential transport of a wide range of cargos, but also to completely prevent fouling[19]. Most interestingly, micropores between air sacs in the lung are filled with liquid that has been proposed to reversibly reconfigure inside the pore to create an open, liquid-lined pathway in response to pressure gradients[20].

Figure 1 contrasts the gating mechanisms in a conventional pore and in a liquid-filled pore. In the case of conventional nano- or micropores (Fig. 1a), gases will flow through passively regardless of pore shape and surface chemistry, whereas liquids will enter the pore once the applied pressure reaches a critical value dictated by the balance of surface interactions, pore geometry and surface tension[21–23]. If the pores are filled with a strongly wetting liquid that completely seals them and forms a contiguous coating along the adjacent surface (Fig. 1b), gases and liquids must deform the interface of the pore-filling liquid to enter the pore and will require different pressure thresholds to do so. As long as the pore-filling liquid's affinity for the solid is stronger than that of the transport substance, the pore liquid will part to form an open, liquid-lined pathway while remaining adherent to the pore walls and adjacent surfaces, such that the transport substance, as long as it is immiscible, will flow through without contacting any solid surfaces. Unlike with bare pores, the transport substance will thus contact only the liquid in either the open or the closed state, preventing fouling both inside[24] and around[25] the pore. Because this dynamic gating mechanism involves structural reconfiguration, rather than expulsion, of the pore liquid, the pore will stay open only as long as the transport substance is flowing and will be thermodynamically primed to close as soon as the pressure drops below the threshold.

This rationale can be used to design gated transport systems having a wide variety of pore sizes, pore geometries, surface chemistries and gating liquids. We illustrate this by using membrane materials with different pore structures (Fig. 2a and Supplementary Fig. 1) and chemistries, ranging from hydrophobic polytetrafluoroethylene (PTFE), poly(vinylidene fluoride) and polypropylene (Supplementary Table 1) to hydrophilic nylon. Air flows through all of these materials in their unmodified state at zero pressure, but adding a gating liquid creates a substantial critical gating pressure that has a distinct value for each membrane (Fig. 2b). Because the liquid-gated pore can open and close in response to different conditions and transport substances, gas and liquid flows can be differentially controlled in a single system. For example, filling PTFE pores with a low-surface-energy liquid simultaneously generates

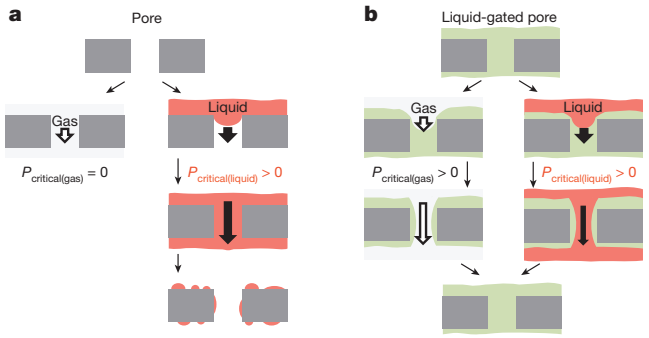

Figure 1 | Hypothesis for gating a pore by liquid reconfiguration. **a**, For a solid nano- or micropore (significantly larger than the molecular scale), transport of gases (light grey) is uncontrolled and occurs even at zero pressure, whereas transport of liquids (red) depends on the meniscus formation defined by the interactions with the solid surface and therefore occurs at specific finite pressure. The system is prone to fouling. **b**, If the pore is filled with a stably held liquid (green), flow of both gases and liquids will be gated by pressure-induced deformation of the gating liquid surface. In the open state, the gating liquid will reversibly reconfigure to form a liquid-lined pore. Each transport substance will have a specific critical pressure based on its ability to overcome the capillary pressure at the liquid-gas or liquid-liquid interface, and the liquid-lined pore will prevent contact with the solid. When the pressure is released, a non-fouled pore returns to its original liquid-filled state. The liquid-based gating mechanism provides a unified strategy for selective, responsive, tunable and antifouling multiphase transport.

[1]School of Engineering and Applied Sciences, Harvard University, Cambridge, Massachusetts 02138, USA. [2]Wyss Institute for Biologically Inspired Engineering, Harvard University, Cambridge, Massachusetts 02138, USA.

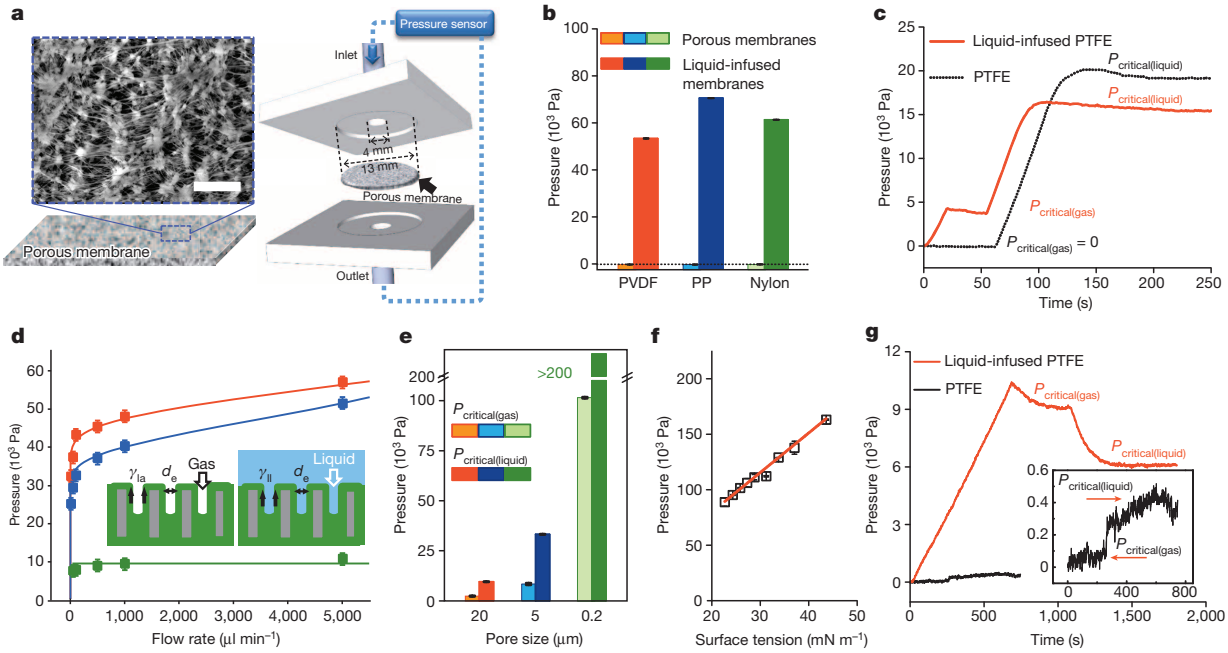

Figure 2 | Design and rational tuning of gating systems with differentially controlled gas and liquid transport. **a**, Left: scanning electron micrograph of a typical porous membrane. Scale bar, 5 μm. Right: sketch of the pressure measurement set-up. **b**, Critical pressure required for gas to flow through porous materials of various chemistries and pore structures (average pore size, 0.45 μm), with and without a gating liquid. For each material, $P_{critical(gas)} = 0$ without the gating liquid and $P_{critical(gas)} > 0$ with the gating liquid. PP, polypropylene; PVDF, poly(vinylidene fluoride). **c**, Liquid-based gating creates different critical pressures for gas and water within a single system. Importantly, the critical pressure for water transport through a liquid-filled membrane is less than that for transport through the same membrane without liquid. **d**, The predictive model (lines) agrees with experimentally obtained critical pressures (squares) over a range of flow rates for air through liquid-gated pores (green), water through liquid-gated pores (blue), and water through pores without a liquid gate (red). Inset, schematic model for determining critical pressure for gases and liquids. In both cases, the gating pressure is a function of the pore geometry and interfacial (gas–liquid or liquid–liquid) tension. **e**, Differential tuning of absolute and relative critical pressures for air and water to flow through liquid-gated pores with different pore sizes. **f**, Systematic tuning of the gating threshold for air transport by infusing porous nylon membranes with a series of gating liquids of different surface tensions, achieved by mixing water and ethanol in different ratios. **g**, Critical pressures for air (black) and ethanol (red) through liquid-gated pores. The difference in interfacial tensions leads to an unusual situation in which the critical pressure for liquid is lower than that for gas. Inset: without the gating liquid, the critical pressures for both air and ethanol are negligible. All error bars, 1 s.d.

a gating pressure for air and alters—in this case lowers—the critical pressure for water, such that both substances can be transported through the membrane in succession according to their distinct thresholds (Fig. 2c and Supplementary Fig. 2).

Gating for gases and liquids is expected to occur via the same capillary mechanism, where the critical pressure will be the pressure needed to deform the surface of the pore-filling liquid (Fig. 2d, insets). For a gas, the pressure that must be overcome is the Laplace pressure, $4\gamma_{la}/d_e$, where γ_{la} is the surface tension of the pore-filling liquid and d_e is the average effective pore size[26]. These parameters are sufficient to predict the experimentally observed critical pressure for air in a 5 μm porous membrane infused with a low-surface-energy liquid (Fig. 2d, green). For a liquid, the gating pressure will depend on d_e and on the liquid–liquid interfacial tension γ_{ll}; in fact, this relationship[27] is used to characterize membrane porosity by observing the irreversible expulsion of the pore-filling liquid[26,28]. But in our case, where we aim for the gating liquid to reversibly reconfigure in place so that the transport liquid continuously flows through a liquid-lined pore, the working pressure will also depend on the flow rate Q and viscosity μ of the transport fluid[29], as $\Delta P \propto Q\mu/k$. In this expression, k is the permeability of the membrane, which is related to the pore structure and size and also depends on the transmembrane pressure or flow rate[29,30]:

$$k = \frac{\Phi}{32\tau^2} \int_{2\gamma_{ll}/\Delta P}^{\infty} \frac{X^2}{\sigma\sqrt{2\pi}} e^{-(X-d)^2/2\sigma^2} \, dX$$

Here Φ is the porosity, τ the tortuosity, d the mean pore size and σ the standard deviation of a porous membrane with distributed pore sizes (Supplementary Information). This relationship accurately predicts the gating pressure for water at a series of flow rates, both with and without the pore-filling liquid (Fig. 2d, blue and red), and allows us to quantitatively determine how the performance of the system depends on the pore size, geometry and gating liquid properties (Supplementary Fig. 3 and Supplementary Tables 2 and 3).

We can use a variety of membranes with different pore sizes to tune the absolute and relative critical pressures for gases and liquids over at least two orders of magnitude, from less than 10 kPa to more than 200 kPa (Fig. 2e and Supplementary Fig. 4). For a given membrane material and pore size, the gating pressure is finely tuned by using pore-filling liquids with systematically varying surface tensions (Fig. 2f, Supplementary Fig. 5 and Supplementary Table 4). We can even adjust the system so that the critical pressure for air exceeds that for the liquid, in this case ethanol (Fig. 2g). In all cases, the observed gating thresholds are independent of whether gas or liquid is flowed first (Supplementary Fig. 6), and are stable over time and after cyclic alteration of gas and liquid (Supplementary Fig. 7).

This combination of differential tunability and reversible opening and closing enables fast and repeatable control over multiphase flows in both microfluidic and macrofluidic systems by simply adjusting the system pressure. For example, we can produce distinct air–water streams by incorporating a liquid-gated porous membrane into a port in a microfluidic channel and setting the critical pressures for air and water to 2.3 and 9.8 kPa, respectively (Fig. 3a, Supplementary Figs 8–11 and Supplementary Video 1). Below 2.3 kPa, neither substance flows through the port (Fig. 3a, first panel). Between the two critical pressures, only air flows through the port, and gas-free water continues past it (Fig. 3a,

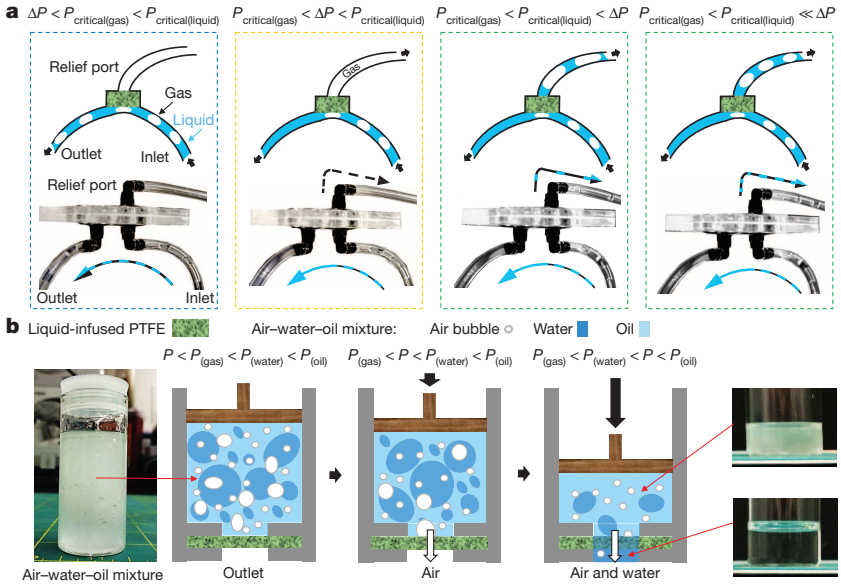

Figure 3 | Sorting of multiphase mixtures by liquid-gated pores. **a**, Rapid pressure-tunable sorting of multiphase flows in a microfluidic system. Top: sketches; bottom: snapshots of experiment. A liquid-infused porous material incorporated into a port along a microfluidic channel enables a series of distinct pressure-dependent scenarios for a mixed gas–liquid flow. In the sketches, the membrane is shown in green and the transported liquid is shown in blue; the blue arrows depict the transport of liquid, dashed black and blue arrows correspond to the transport of a mixed gas–liquid phase, and dashed black and white arrows depict the transport of gas only. First panel: at pressures below both $P_{critical(gas)}$ and $P_{critical(liquid)}$, nothing flows through the port. Second panel: above $P_{critical(gas)}$ and below $P_{critical(liquid)}$, only the gas flows through the port, and degassed liquid continues through the channel beyond the port. Third and fourth panels: at pressures above both $P_{critical(gas)}$ and $P_{critical(liquid)}$, both phases cross the port and only liquid continues through the channel beyond the port. Note that above both critical pressures, the liquid/gas ratio of the mixture that crosses the port increases with increasing pressure. Data shown are for an alternating air–liquid flow, with $P_{critical(gas)} = 2.3$ kPa and $P_{critical(liquid)} = 9.8$ kPa. **b**, A three-phase mixture of air, water and crude oil is progressively separated by the liquid-infused porous membrane.

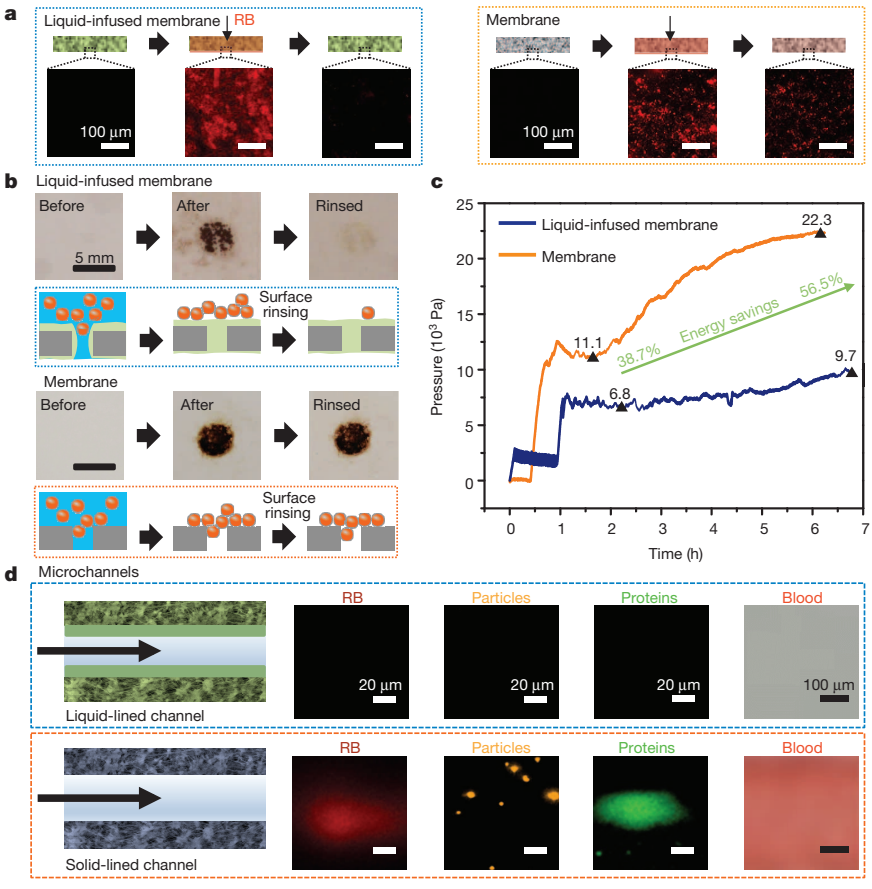

Figure 4 | Antifouling transport and separation of complex substances. **a**, Real-time confocal images of a liquid-infused porous material (left) or of the porous material without the gating liquid (right) before, during and after flowing an aqueous solution of rhodamine B dye (RB). Detention of dye after flow is observable only in the PTFE membrane without the gating liquid. **b**, Flowing a suspension of 4-benzoylamino-2,5-diethoxybenzenediazonium chloride hemi(zinc chloride) salt particles (1,000 μl min^{-1}) through a liquid-infused porous material (top) leaves salt particles suspended on the liquid surface after the pore closes (top, centre), and the particles are easily collected by a gentle surface rinse (top, right). The bare membrane (bottom) traps the salts both in and around the pores (bottom, centre) and resists repeated rinsing (bottom, right). **c**, The pressure required to transport a suspension of 4-benzoylamino-2,5-diethoxybenzenediazonium chloride hemi(zinc chloride) salt particles in water through a liquid-infused PTFE membrane is initially 38.7% lower than the pressure required for transport through the bare membrane. This percentage difference increases to about 56.5% after 4.5 h operation at a flow rate of 50 μl min^{-1} owing to fouling of the bare membrane. The energy saving rate is $(P_{PTFE} - P_{PTFE–Krytox\ 103})/P_{PTFE}$, where Krytox 103 is the pore-filling liquid. **d**, A liquid-lined PTFE microchannel resists fouling (top) by an RB solution, suspended microparticles and a protein solution (fluorescent images) and by blood (optical image), whereas fouling residue is observed inside the bare PTFE channel for each substance (bottom).

second panel). Above 9.8 kPa, both air and water flow through the port (Fig. 3a, third panel), with their precise balance responding to graded pressure changes (Fig. 3a, fourth panel) because pressure increases the flow rate through the port significantly for liquids but only negligibly for gases (Supplementary Information and Supplementary Fig. 12). The robustness of the gating behaviour indicates that the pores can sustain many rapid opening–closing cycles while remaining faithful to the original gating pressures, allowing the system to be operated continuously for at least several days (Supplementary Video 1). We also explore more complex fluid handling using these principles: by setting a distinct threshold for each component of a three-phase gas–liquid–liquid mixture, we use pressure to actively adjust and control selective fluid flow through the liquid-gated membrane to collect the different phases while preventing the escape of any component (Fig. 3b and Supplementary Fig. 13).

The liquid-gating strategy further suppresses fouling, as illustrated by the real-time confocal images in Fig. 4a, which show that a rhodamine B dye solution leaves no trace on liquid-gated membranes once the flow stops, whereas bare pores retain substantial dye (Supplementary Figs 14–15). Lining the membrane pores and outer surfaces with liquid thus indeed prevents the transport substance from contacting the solid (Fig. 1), enabling the separation of suspensions containing particles larger than the pore diameter without risk of fouling. This is further illustrated in Fig. 4b, where salt particles are found only on top of the closed pores following flow and are collected by a gentle surface rinse; the bare membrane traps the particles in and around the pores and resists repeated rinsing (Supplementary Fig. 16). The integration of antifouling behaviour and pressure-controlled flow properties in one system not only provides the flexibility to have a lower working pressure for liquid transport than with conventional membranes, but also avoids the common problem of working pressure build-up caused by pore clogging and uncontrolled fouling. The combination of these effects can lead to significant energy savings in long-term operation (Fig. 4c; see Supplementary Information for discussion).

A liquid lining prevents fouling not only inside nano- and micropores, but also in much longer microfluidic channels. As illustrated in Fig. 4d, a microfluidic channel lined with a liquid-filled porous membrane shows no retention of rhodamine B, fluorescent microparticles, fluorescent protein or blood, whereas state-of-the-art but conventional non-fouling microfluidic channels retain substantial residue. By using liquid-lined channels and pores, it should therefore be possible to design microfluidic systems that resist fouling and enable tunable gated flow of complex multiphase substances.

The dynamic reconfiguration of a liquid lining as a means to reversibly open and close membrane pores provides an attractive and tunable gating mechanism that integrates chemical and physical selectivity for gas- and liquid-phase transport substances with non-fouling behaviour and energy-efficient operation. We anticipate that these capabilities, combined with the longevity of the membrane systems, the range of materials and geometries that can be used in their construction, and their applicability to both macro- and microfluidic operation, will be of benefit in fields ranging from water treatment and biomedical fluid processing to 3D printing, microscale reactor operation and beyond.

Received 22 June 2014; accepted 15 January 2015.

1. Chen, P. C. & Xu, Z. K. Mineral-coated polymer membranes with superhydrophilicity and underwater superoleophobicity for effective oil/water separation. *Sci. Rep.* **3,** 2776 (2013).
2. Holt, J. K. *et al.* in *Proc. 4th IEEE Conf. Nanotechnol.* 110–112 (IEEE, 2004).
3. Peng, X. S., Jin, J., Nakamura, Y., Ohno, T. & Ichinose, I. Ultrafast permeation of water through protein-based membranes. *Nature Nanotechnol.* **4,** 353–357 (2009).
4. Paven, M. *et al.* Super liquid-repellent gas membranes for carbon dioxide capture and heart-lung machines. *Nature Commun.* **4,** 2512 (2013).
5. Faulkner-Jones, A. *et al.* Development of a valve-based cell printer for the formation of human embryonic stem cell spheroid aggregates. *Biofabrication* **5,** 015013 (2013).
6. Oh, K. W. & Ahn, C. H. A review of microvalves. *J. Micromech. Microeng.* **16,** R13–R39 (2006).
7. Kargov, A. *et al.* in *Proc. IEEE 9th Int. Conf. Rehabilitation Robotics* 182–186 (IEEE, 2005).
8. Edwards, D. A. *et al.* Large porous particles for pulmonary drug delivery. *Science* **276,** 1868–1872 (1997).
9. Kralj, J. G., Sahoo, H. R. & Jensen, K. F. Integrated continuous microfluidic liquid-liquid extraction. *Lab Chip* **7,** 256–263 (2007).
10. Karlsson, J. M. *et al.* Active liquid degassing in microfluidic systems. *Lab Chip* **13,** 4366–4373 (2013).
11. Ulbricht, M. Advanced functional polymer membranes. *Polymer* **47,** 2217–2262 (2006).
12. Lin, N. H., Kim, M. M., Lewis, G. T. & Cohen, Y. Polymer surface nanostructuring of reverse osmosis membranes for fouling resistance and improved flux performance. *J. Mater. Chem.* **20,** 4642–4652 (2010).
13. Powell, M. R., Cleary, L., Davenport, M., Shea, K. J. & Siwy, Z. S. Electric-field-induced wetting and dewetting in single hydrophobic nanopores. *Nature Nanotechnol.* **6,** 798–802 (2011).
14. Yameen, B. *et al.* Ionic transport through single solid-state nanopores controlled with thermally nanoactuated macromolecular gates. *Small* **5,** 1287–1291 (2009).
15. Wen, Y. Q. *et al.* DNA-based intelligent logic controlled release systems. *Chem. Commun.* **48,** 8410–8412 (2012).
16. Adrus, N. & Ulbricht, M. Novel hydrogel pore-filled composite membranes with tunable and temperature-responsive size-selectivity. *J. Mater. Chem.* **22,** 3088–3098 (2012).
17. Nair, R. R., Wu, H. A., Jayaram, P. N., Grigorieva, I. V. & Geim, A. K. Unimpeded permeation of water through helium-leak–tight graphene-based membranes. *Science* **335,** 442–444 (2012).
18. Stroock, A. D., Pagay, V. V., Zwieniecki, M. A. & Holbrook, N. M. The physicochemical hydrodynamics of vascular plants. *Annu. Rev. Fluid Mech.* **46,** 615–642 (2014).
19. Peleg, O. & Lim, R. Y. H. Converging on the function of intrinsically disordered nucleoporins in the nuclear pore complex. *Biol. Chem.* **391,** 719–730 (2010).
20. Namati, E., Thiesse, J., de Ryk, J. & McLennan, G. Alveolar dynamics during respiration: are the pores of Kohn a pathway to recruitment? *Am. J. Respir. Cell Mol. Biol.* **38,** 572–578 (2008).
21. Winther-Jensen, B., Winther-Jensen, O., Forsyth, M. & Macfarlane, D. R. High rates of oxygen reduction over a vapor phase-polymerized PEDOT electrode. *Science* **321,** 671–674 (2008).
22. Mohns, J. & Kunnecke, W. Flow-analysis with membrane separation and time-based sampling for ethanol determination in beer and wine. *Anal. Chim. Acta* **305,** 241–247 (1995).
23. Liu, C. C., Thompson, J. A. & Bau, H. H. A membrane-based, high-efficiency, microfluidic debubbler. *Lab Chip* **11,** 1688–1693 (2011).
24. Yusko, E. C. *et al.* Controlling protein translocation through nanopores with bio-inspired fluid walls. *Nature Nanotechnol.* **6,** 253–260 (2011).
25. Wong, T. S. *et al.* Bioinspired self-repairing slippery surfaces with pressure-stable omniphobicity. *Nature* **477,** 443–447 (2011).
26. Mietton-Peuchot, M., Condat, C. & Courtois, T. Use of gas-liquid porometry measurements for selection of microfiltration membranes. *J. Membr. Sci.* **133,** 73–82 (1997).
27. Zhang, C. Y., Oostrom, M., Wietsma, T. W., Grate, J. W. & Warner, M. G. Influence of viscous and capillary forces on immiscible fluid displacement: pore-scale experimental study in a water-wet micromodel demonstrating viscous and capillary fingering. *Energy Fuels* **25,** 3493–3505 (2011).
28. Germic, L. *et al.* Characterization of polyacrylonitrile ultrafiltration membranes. *J. Membr. Sci.* **132,** 131–145 (1997).
29. Biot, M. A. General theory of three-dimensional consolidation. *J. Appl. Phys.* **12,** 155–164 (1941).
30. Purcell, W. R. Capillary pressures - their measurement using mercury and the calculation of permeability therefrom. *J. Petrol. Technol.* **1,** 39–48 (1949).

Supplementary Information is available in the online version of the paper.

Acknowledgements This work was supported in part by the Advanced Research Projects Agency-Energy (ARPA-E), US Department of Energy, under award number DE-AR0000326. We thank M. Aizenberg, R. T. Blough and X. Y. Chen for discussions; A. B. Tesler for assistance with the scanning electron microscopy; and T. S. Wong, B. D. Hatton and R. A. Belisle for assistance with antifouling experiments.

Author Contributions X.H. and J.A. designed the liquid-infused porous materials and the experiments. X.H. and M.K. carried out the experiments. All authors analysed data. Y.H. built the mathematical model. All authors interpreted data and wrote the paper.

Author Information Reprints and permissions information is available at www.nature.com/reprints. The authors declare no competing financial interests. Readers are welcome to comment on the online version of the paper. Correspondence and requests for materials should be addressed to J.A. (jaiz@seas.harvard.edu).